Cross section determination of ^{27}Al(n,2n)^{26}Al reaction induced by 14 MeV neutrons uniting with D-T neutron activation and AMS techniques*

Xian-Lin Yang,[1,2] Chang-Lin Lan,[1,2,†] Yu-Ting Wei,[1,2] Yi Zhang,[1,2] Gong Jiang,[1,2] Bo Xie,[1,2] Yu Liu,[3] Hong-Tao Shen,[4,‡] and Xiao-Jun Sun[4]

[1]*School of Nuclear Science and Technology, Lanzhou University, Lanzhou 730000, China*
[2]*MOE Frontiers Science Center for Rare Isotopes, Lanzhou University, Lanzhou 730000, China*
[3]*State Key Laboratory of Environmental Geochemistry, Institute of Geochemistry, Chinese Academy of Sciences, Guiyang 550081, China*
[4]*Guangxi Key Laboratory of Nuclear Physics and Nuclear Technology, Guangxi Normal University, Guilin 541004, China*

Aluminum is the primary structural material in nuclear engineering, and its cross-section induced by 14 MeV neutrons is of great significance. To address the issue of insufficient accuracy for the ^{27}Al(n,2n)^{26}Al reaction cross-section, the activation method and accelerator mass spectrometry (AMS) technique were used to determine the ^{27}Al(n,2n)^{26}Al cross-section, which could be used as a D-T plasma ion temperature monitor in fusion reactors. At the China Academy of Engineering Physics (CAEP), neutron activation was performed using a K-400 neutron generator produced by the T(d,n)^{4}He reaction. The ^{26}Al/^{27}Al isotope ratios were measured using the newly installed GYIG 1 MV AMS at the Institute of Geochemistry, Chinese Academy of Sciences. The neutron flux was monitored by measuring the activity of ^{92m}Nb produced by the ^{93}Nb(n,2n)^{92m}Nb reaction. The measured results were compared with available data in the experimental nuclear reaction database, and the measured values showed a reasonable degree of consistency with partially available literature data. The newly acquired cross-sectional data at 12 neutron energy points through systematic measurements clarified the divergence, which has two different growth trends from the existing experimental values. The obtained results are also compared with the corresponding evaluated database, and the newly calculated excitation functions with TALYS-1.95 and EMPIRE-3.2 codes, the agreement with CENDL-3.2, TENDL-2021 and EMPIRE-3.2 results are generally acceptable. A substantial improvement in the knowledge of the ^{27}Al(n,2n)^{26}Al reaction excitation function was obtained in the present work, which will lay the foundation for the diagnosis of the fusion ion temperature, testing of the nuclear physics model, and evaluation of nuclear data, etc.

Keywords: 14 MeV neutron; ^{27}Al(n,2n)^{26}Al; cross section; AMS

I. INTRODUCTION

Its high strength-to-weight ratio and relatively low activation rate make aluminum one of the most attractive materials for many structural applications, such as fusion reactors, accelerator subcritical systems, and Generation IV reactors [1, 2]. The cross-section of aluminum is of great significance not only for its general applicability in testing nuclear models but also for the estimation of displacement damage in A1-metal alloys and the radioactivity of the long-lived ground state ^{26}Al ($T_{1/2}$ =7.17 $\times$ 10^5 a) that produced 1808.65 keV gamma ray [3]. In addition, a high threshold (13.5 MeV) and a dramatic increase in the ^{27}Al(n,2n)^{26}Al reaction cross-section with neutron energy in the 14 MeV region plays an essential role in the monitoring of ion temperature in a D-T fusion plasma, as pointed out by Smither and Wallner et al. [4, 5].

However, owing to the long half-life of ^{26}Al(Ma) and the small cross-section (mb) of the ^{27}Al(n,2n)^{26}Al reaction near the threshold, it is challenging to quantify the cross-section of the ^{27}Al(n,2n)^{26}Al reaction using gamma spectrometry. As the most sensitive measurement technology for ^{26}Al to date [6], accelerator mass spectrometers (AMS) have significantly shortened the irradiation and measurement time of the ^{27}Al(n,2n)^{26}Al reaction channel and effectively improved the accuracy of the data. In particular, accelerator mass spectrometers have been widely used to measure the cross sections and half-lives of nuclear reactions associated with long-lived nuclides [7–11]. Nevertheless, cross-sectional measurements of the ^{27}Al(n,2n)^{26}Al reaction are insufficient, and the available data differ significantly, as illustrated in Fig. 1, because of the limitations of single-energy neutron sources and high-precision accelerator mass spectrometers.

The following is a brief overview of the previous ^{27}Al(n,2n)^{26}Al reaction measurement procedure. With the emergence of accelerator mass spectrometry technology, the first measurement of the ^{27}Al(n,2n)^{26}Al cross-section was reported by Smither et al. [4] in 1984; however, these data were not included in the experimental nuclear reaction data (EXFOR). Using a well-shielded germanium detector, Sasao detected 1.809 MeV γ rays following the β decay of ^{26}Al to calculate the ^{27}Al(n,2n)^{26}Al reaction cross-section in 1987 [12]. Although the uncertainty of the neutron energy was mea-

* The authors are thankful to the staff of the K-400 facility at the Chinese Academy of Engineering Physics for their excellent operation of the neutron generator and other support during the experiment. We also thank the assistance provided by Mr. Guo-Qing Zhao for sample preparation and Dr. Yun-chong Fu for the AMS operation at Xi'an AMS center. This work was supported by the Open Project of Guangxi Key Laboratory of Nuclear Physics and Nuclear Technology (NLK 2022-04), the Central Government Guidance Funds for Local Scientific and Technological Development, China (No. Guike, ZY22096024), National Natural Science Foundation of China (12065003), and Guangxi Key R&D Project (2023AB07029)

† Corresponding author, lanchl@lzu.edu.cn
‡ Corresponding author, shenht@gxnu.edu.cn

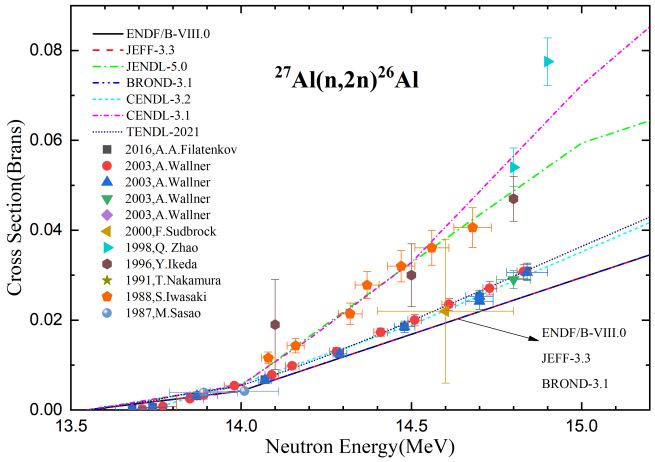

Fig. 1. (Color online) Previous results for the excitation function of the ^{27}Al(n,2n)^{26}Al reaction near threshold.

sured by the ratio of the ^{90}Zr(n,2n)$^{89m+g}$Zr cross-section to the ^{93}Nb(n,2n)^{92m}Nb near 14 MeV, the cross-section error details were not given. In 1988, Iwasaki et al. conducted irradiation for several months using a DT generator. The measurements were performed after approximately one year of cooling. In 1991, 15–34 MeV neutrons were produced by bombarding a 1 mm-thick beryllium target with a 3–5 microamp proton beam. Nakamura et al. [13] provided only high-energy cross-sectional data using the AMS. In 1996, Al samples were irradiated for four days, and γ-ray measurements lasted for more than 1.7 years using a Ge detector with high detection efficiency. The uncertainty of the neutron energy is not given in the original literature, whereas the cross-sectional uncertainty is in the range of 10% to 50%. In 1998, two samples were irradiated with a D-T neutron beam for approximately 20 d. Qiang et al. obtained the first ^{27}Al(n,2n)^{26}Al cross-section at two neutron energy points using a 6 MV AMS [14] in China, and the data were the maximum cross-section in the 14 MeV neutron energy region. In 2000, Sudbrock et al. reported four different reaction cross-section measurements at 14.6 MeV neutron energy via AMS [1]. Although the error of the ^{27}Al(n,2n)^{26}Al reaction in Sudbrock's work is more than 70%, the cross-section also falls within the range of values predicted from the systematics of the (n,2n) reaction cross sections at 14.6 MeV. In 2003, Wallner et al. [5] provided a comprehensive study on the measurement of the ^{27}Al(n,2n)^{26}Al reaction cross-section. At 14.8 MeV, the cross-sectional values of the ^{27}Al(n,2n)^{26}Al reaction are 30% and 40% lower than Y. Ikeda's and Q. Zhao's, respectively. In 2016, A.A. Filatenkov gave results consistent with Wallner's study.

Although the ^{27}Al(n,2n)^{26}Al reaction was carefully measured and evaluated, as shown in Fig. 1, there are still non-negligible discrepancies between the values recommended by the different evaluated nuclear data libraries. The 14 MeV neutron energy region has a 50% difference between the evaluated values [15–18]. The evaluated values of CENDL-3.2 were significantly different from those of CENDL-3.1. Considering the insufficient experimental data, further investigation is required for the evaluated database based on various theoretical models. In conclusion, there are two distribution trends in the existing experimental and evaluation data. Therefore, it is essential to clarify the divergence between the two distribution trends for application.

In the present work, the cross sections for the ^{27}Al(n,2n)^{26}Al reaction in the 14 MeV neutron energy region are determined by utilizing the AMS technique with careful consideration of the experimental background to meet the requirements of nuclear physics and nuclear engineering. After comparing the (n,2n) cross sections of ^{27}Al obtained in the present measurement with the existing data and evaluation values, the new experimental results determined a new excitation function more accurately.

II. EXPERIMENTAL PROCEDURE

A. Neutron source

In the neutron energy range from 13.5 to 15.0 MeV, irradiations were performed at the K-400 neutron generator of the China Academy of Engineering Physics (CAEP). The neutron yield of the K-400 neutron generator is approximately (3–5)$\times 10^{10}$ n/s. The neutrons were produced by a T(d,n)^{4}He reaction with a D^+ beam current of 250 μA. The thickness of the solid tritium-titanium (T-Ti) target used in the generator was 2.5 mg/cm^2, and the energy of the incident D^+ beam was 300 keV. An Au-Si surface barrier detector was installed at 135° with respect to the D^+ beam and at a distance of 100 cm from the T-Ti target for the detection of accompanying particles. The neutron flux was recorded and kept every ten seconds to obtain the neutron flux fluctuation over the entire irradiation period.

B. Samples irradiation and neutron energy

High purity aluminum (0.5 mm, 99.999% purity) foil was sandwiched between natural zirconium (0.1 mm, 99.5% purity) and niobium (0.1 mm, 99.95% purity) foils. The first set of foils was tailored to form a round disk with a diameter of 20 mm. Four sandwich samples were placed approximately 5.0 cm away from the T-Ti target relative to the deuteron beam's incident angles of 0°, 30°, 60° and 100°. The dimensions of the second set of foils were 0.5 cm in width and about 4 cm in length, which were in arc shape and placed about 3.0 cm away from the T-Ti target and about 60° to 135° relative to the deuterium ion incident direction. The schematic diagram of experimental geometry is shown in Fig. 2. The second set of foils was cut into 8 squares with a side length of 0.5 cm after the irradiation. The precise weight of each foil was determined with an analytic balance ($\pm$0.01 mg) after irradiation.

Two sets of aluminum samples placed at different locations from the tritium titanium target were irradiated for 20 h. It is essential to accurately determine the neutron energy for cross-sectional measurements, particularly those near the thresh-

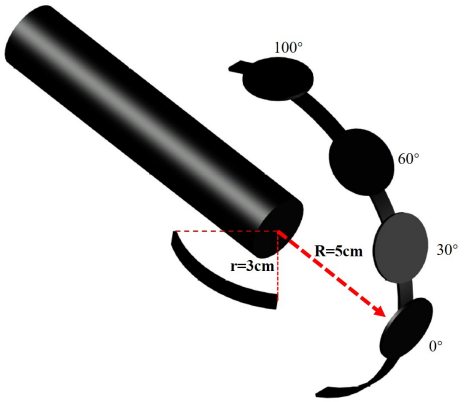

Fig. 2. (Color online) Schematic diagram of experimental geometry.

old. The neutron energies were measured using the Zr-Nb method [19, 20]. As a cross-check, the neutron energies of the first set of foils were calculated using an improved theoretical method, which was used to determine the mean D-T neutron energies in a large solid angle sample [21, 22]. There are two sets of parameters for the Zb-Nb method, and the neutron energies were calculated using these two sets of parameters. The mean value of the two results was used to determine the final neutron energy, as described in Sect. V. The uncertainties in the incident neutron energies given above are the quadratic roots of the summed square of the uncertainties caused by the results of the activity measurements for Zr and Nb foils [23]. The entire available energy range starts from the threshold of the (n,2n) reaction to approximately 14.90 MeV. It is reasonable to suppose that the scattered neutrons from the target construction and the surrounding environment are insignificant because of the high threshold of the ^{27}Al(n,2n)^{26}Al reaction. In addition, the cross-section of ^{93}Nb(n,2n)^{92m}Nb was used as a standard to monitor the integral neutron flux for all samples. The relevant nuclear parameters for ^{93}Nb(n,2n)^{92m}Nb and ^{90}Zr(n,2n)$^{89m+g}$Zr are listed in Table 1.

C. Measurement of ^{92m}Nb and $^{89m+g}$Zr activity

After irradiation, there was a cooling period. Then, the activities of those Nb and Zr samples were determined using an HPGe γ-ray detector(as shown in Fig. 3). Before Nb and Zr samples were measured, a series of standard point sources (^{22}Na, ^{60}Co,^{133}Ba, ^{137}Cs, and ^{152}Eu) of known activity were used to determine the absolute full-energy peak efficiency of a lead-shielded high-purity germanium detector (ORTEC, USA). The radioactivity of the reaction product was determined via the well-calibrated HPGe detector with a relative efficiency of 68% and an energy resolution of 1.82 keV FWHM at 1.33 MeV. The distance between the sample and the detector was 5.0 cm. Efficiency calibration was determined using point-like standard gamma-ray sources. The detection efficiencies for the point source placed at a distance of 5.0 cm from the detector were determined using Eq. (1)

$$\epsilon_{\rm p} = \frac{C'}{A_0 \exp^{-\lambda t} \Delta t I_\gamma} \tag{1}$$

where C' is the count number of the point source during the counting time (Δt), A_0 is the source activity at the time of manufacturing, t is the time elapsed from the date of manufacturing to the start time of counting, γ is the decay constant, and I_γ is the decay γ intensity.

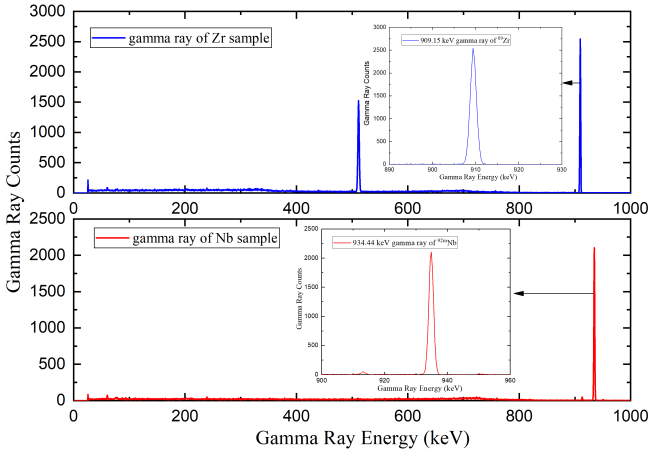

Fig. 3. (Color online) Typical γ-ray spectrum in zirconium and niobium sample.

The efficiency values obtained for the characteristic γ-ray energies of the point source are described using an exponential function [24] expressed in Eq. (2). The detector efficiency for the characteristic γ-ray energies of ^{92m}Nb and $^{89m+g}$Zr was then obtained using Eq. (2). The detector efficiency uncertainties of ^{92m}Nb and $^{89m+g}$Zr were obtained by evaluating the uncertainties of the standard sources.

$$\epsilon(E) = \epsilon_0 \exp(-E/E_0) + \epsilon_c \tag{2}$$

The fitting parameter values are 2.53 (ϵ_0), 264.14 (E_0), and 0.33 (ϵ_c), respectively. The value of R^2 is 0.992.

D. ^{26}Al measurement at GYIG 1 MV AMS

Because ^{26}Al has a half-life of millions of years, it is difficult to measure ^{26}Al with high-purity germanium; therefore, an ultrasensitive AMS was needed to measure ^{26}Al in the present work. As a dedicated accelerator mass spectrometer, the GYIG 1 MV AMS instrument has been installed at the Institute of Geochemistry, Chinese Academy of Sciences since 2022 and was designed for multinuclide measurements such as ^{10}Be, ^{14}C, ^{26}Al, and ^{41}Ca. After the installation was completed, the relevant acceptance and commissioning works were also completed. The present study was performed using a 1 MV AMS. A schematic of the GYIG AMS facility

TABLE 1. Associated decay data of ^{93}Nb(n,2n)^{92m}Nb, ^{90}Zr(n,2n)$^{89m+g}$Zr and ^{27}Al(n,2n)^{26}Al

Reaction	Abundance of target isotope η (%)	Q value (MeV)	Half-life of product $T_{1/2}$	γ-ray energy (keV)	γ-ray intensity I_γ (%)
^{93}Nb(n,2n)^{92m}Nb	100	-8.831	(10.15 ± 0.02) d	934.44	99.15 ± 0.04
^{90}Zr(n,2n)$^{89m+g}$Zr	51.45	-11.965	(78.41 ± 0.12) h	909.15	99.05 ± 0.03
^{27}Al(n,2n)^{26}Al	100	-12.275	$(7.14 \pm 0.24) \times 10^5$ a	1808.65	99.76 ± 0.04

(model 3SDH-1 Pelletron) is shown in Fig. 4 [25], which mainly includes a cesium sputter negative ion source, a low-energy injection system (electrostatic analyzer and LE magnet), a tandem accelerator, a high-energy analysis system (HE analyzing magnet and electrostatic analyzer), and an energy-sensitive detector [26, 27].

Al_2O_3 was chosen as the proper sputter material. After neutron activation, approximately 0.08 g of aluminum foil was weighed and dissolved in 5 ml of hydrochloric acid (4.5 M) to ensure a uniform mixture of the irradiated sample material. The solutions were diluted with deionized water to 20 mL, respectively. The pH of the solution was adjusted by ammonium hydroxide to 9. A saturated ammonium oxalate solution was added to precipitate aluminum as aluminum hydroxide ($Al(OH)_3$). The $Al(OH)_3$ precipitate was separated by centrifugation at 10000 rpm for 5 min, washed once with saturated ammonium oxalate solution, and rinsed twice with deionized water. The aluminum hydroxide precipitate was transferred to a ceramic crucible. The sample was dried at 60 °C and then heated to 900 °C in a muffle furnace to obtain aluminum oxide powder. After mixing with Ag powder (Mass: Mass=1:1), the prepared samples were pressed into a copper holder, which acted as the cathode in the cesium sputtering negative-ion source, capable of holding 40 cathodes of solid samples [28, 29].

Before the measurement of ^{26}Al, the pilot $^{27}Al^-$ beam was injected into the accelerator after being selected by the injection magnet, and the current of $^{27}Al^-$ was 0.1–1 μA. Because the electron affinity of aluminum is relatively low, the intensity of the $^{27}Al^-$ current from the cesium sputtering negative ion source is insufficient compared to C^- and BeO^- in this machine. Fortunately, Mg^- ions are unstable; thus, isobaric interference is insignificant in the ^{26}Al measurement. The accelerator terminal voltage was set to 0.41 MV, and negative ions were accelerated in the first part of the accelerator. After passing through argon gas at a pressure of 27 Torr, the negative ions were stripped into positive ions with different charge states via collisions and Coulomb breakups and then accelerated in the second part of the accelerator. $^{27}Al^{1+}$ particles were chosen by high-energy analysis system. The beam transmission was approximately 30%, which is the ratio of the ^{27}Al current measured in the Faraday cups before and after passing through the high-energy magnet. After the $^{27}Al^{1+}$ ions reached the Faraday cup before reaching the detector, all parameters were adjusted to fit the ^{26}Al beam transport. Then, the sequential injection of ^{27}Al and ^{26}Al is achieved with a magnet bias supply coupled to the 'bouncer magnet.' The current of the $^{27}Al^{1+}$ ion was integrated at the offline Faraday cup, whereas the radioisotope ^{26}Al was measured using an ionization chamber, which provides high resolution in the energy measurement [30]. Under the influence of the sample preparation level, mixing uniformity with the conductive medium, and sample bombardment degree in the ion source, the multiple measurement current value of $^{27}Al^{1+}$ in a high-energy Faraday cup can fluctuate between tens and hundreds of nA, and the ^{26}Al count follows the same proportion. Consequently, the ^{26}Al/^{27}Al ratio measured between different rounds exhibited little deviation(as shown in Fig. 5). Because AMS is a relative measurement, the standard sample, processing the blank sample, and unknown sample should be measured sequentially. Meanwhile, the raw ratio results were subtracted from the processing blank value and normalized to the standard sample nominal value.

To validate the performance of the newly installed instrument, a series of standard samples with different gradients and blank samples were used. The ratio of the blank samples was less than 4×10^{-15}. The ratios of the Al standard (5.00×10^{-11}) were reproduced to be better than 1% (as shown in Fig. 6). To measure the (n,2n) cross-section, the raw ratios(before normalization) of ^{26}Al/^{27}Al are between 6×10^{-15} and 10^{-13}, which are much larger than the machine background of ^{26}Al/^{27}Al at the GYIG 1 MV AMS. To verify the measurement results of the GYIG 1 MV AMS, four samples and one blank sample were sent to the Xi'an Accelerator Mass Spectrometry Center. The measurement standard for ^{26}Al/^{27}Al is 1.065×10^{-11} in Xi'an and the background is 4.71×10^{-11} [30]. The values of the four irradiated samples were between 1.77×10^{-11} and 2.09×10^{-11}, which is in good agreement with the results of GYIG 1 MV AMS.

III. DATA ANALYSIS

The experimental cross-section σ_{expt} for the ^{27}Al(n,2n)^{26}Al reaction can be determined using Eq. (3) [27]:

$$\sigma_{\text{expt}} = \frac{N_{26}}{N_{27}} \frac{1}{\Phi_{\text{total}}} \tag{3}$$

The ratio ^{26}Al/^{27}Al was determined by AMS, as shown in Table 3, and Φ_{total} is the neutron fluence that can be measured using a monitor.

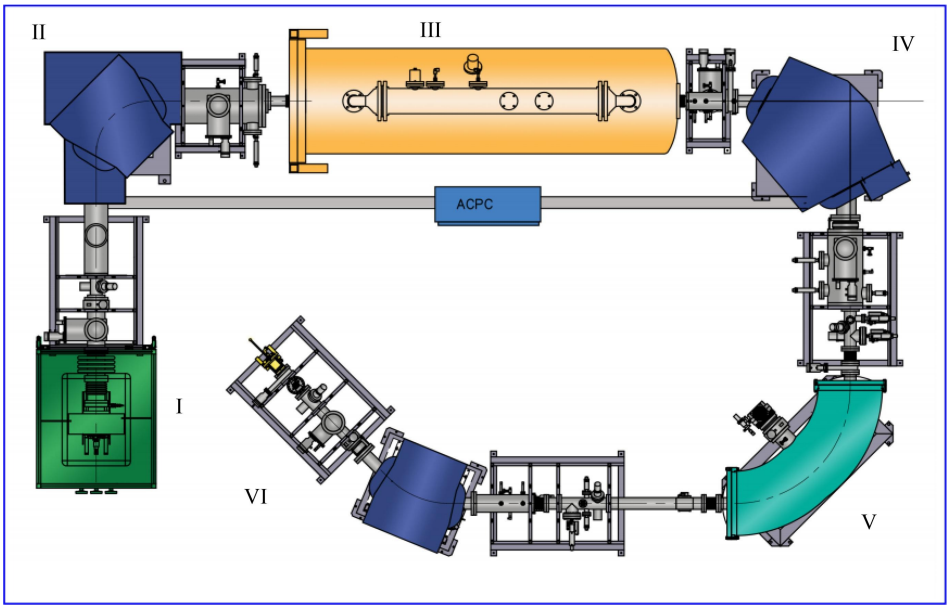

Fig. 4. (Color online) Schematic of the GYIG 1 MV AMS, Model 3SDH-1. I: Ion source II: Sequencer and LE mass analyzer. III: 1 MV Pelletron accelerator and gas stripper. IV: HE analyzing magnet, off-axis Faraday cups. V: The rare isotope beamline (containing the retractable stopper foil, the electrostatic spherical analyzer, the 45° analyzing magnet). VI: Gas ionization detector [25].

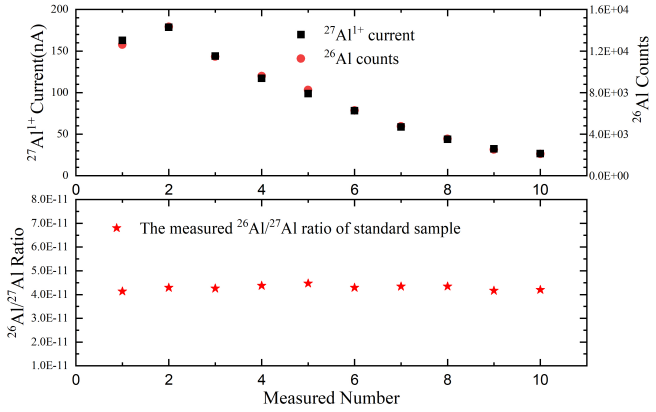

Fig. 5. (Color online) ^{26}Al counting,$^{27}Al^{1+}$ current and $^{26}Al/^{27}Al$ ratio fluctuation among different rounds.

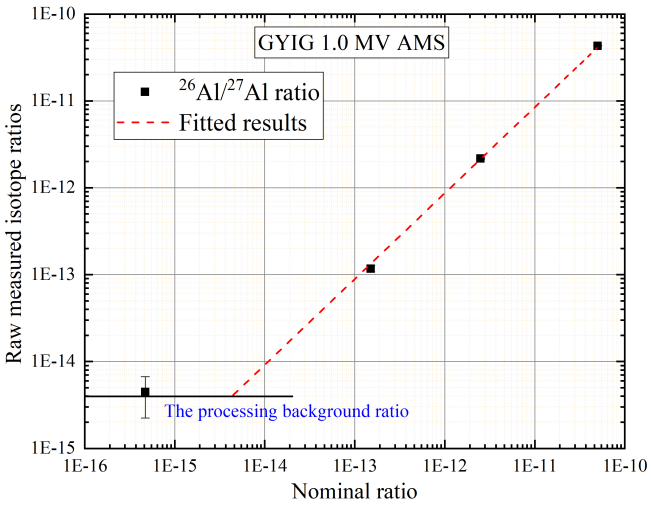

Fig. 6. (Color online) Raw measured isotope ratios for various reference samples versus their nominal values.

A. Neutron fluence

The neutron fluence of the aluminum sample during irradiation was calculated using Eq. (4) [23].

$$\Phi_{\text{total}} = \overline{\phi}T = \frac{FC\lambda A}{MN_A\eta I_\gamma \epsilon KSD\sigma_{\text{m}}}T, \tag{4}$$

where $\overline{\phi}$ is the neutron flux averaged over the sample in the total irradiation time T, σ_{m} is the monitor reaction cross section for ^{93}Nb(n,2n)^{92m}Nb, $S = 1-\exp^{-\lambda T}$ is the growth factor of the residual nuclide, λ is the decay constant of ^{92m}Nb, ϵ is the full-energy peak efficiency of the 934.44 keV γ ray, I_γ is the emission probability of the 934.44 keV γ ray in ^{92m}Nb decay, η is the isotopic abundance of the target nuclide ^{93}Nb, M is the mass of ^{93}Nb, $D = \exp^{-\lambda t_1} - \exp^{-\lambda t_2}$ is the counting collection factor, t_1 (t_2) is the time intervals between the end of irradiation and the start (stop) of counting, A is the atomic weight of ^{93}Nb, C is the measured full-energy peak area, N_{A} is the Avogadro constant, F is the composite correction factor of the activity expressed by Eq. (5), and K is the neutron flux fluctuation factor expressed by Eq. (6) [31–33].

$$F = F_{\text{s}}F_{\text{g}}F_{\text{c}}, \tag{5}$$

where F_{s}, F_{g} and F_{c} are the correction factors for the self-absorption of γ-rays with a given γ energy, counting geom-

etry, and coincidence summing effect of the cascade γ-rays in the investigated nuclide, respectively. In this study, all the samples were measured 50 mm from the surface of the detector. This distance is so large that F_g and F_c are considered negligible [32]. The self-absorption of 934.44 keV γ-ray by 0.1 mm Nb was calculated to be 1.003.

$$K = \frac{\sum_i^L \phi_i (1 - \exp^{-\lambda \Delta t_i}) \exp^{-\lambda T_i}}{\phi S} \quad (6)$$

where L is the number of time intervals, in each of which the accompanying α counts were individually recorded, t_i is the duration of the i^{th} time interval, T_i is the time interval from the end of the i^{th} interval to the end of irradiation, ϕ_i is the relative neutron flux averaged over the sample during t_i (i.e., α counts in t_i), ϕ is the relative neutron flux averaged over the sample in the total irradiation time T (i.e., total α counts in T) [34].

B. Uncertainty analysis

The total uncertainty of the ^{27}Al(n,2n)^{26}Al reaction consists of the monitoring reaction and the AMS contributions. Individual contributions to the total uncertainty are listed in Table 2. The uncertainty in the AMS measurements includes the statistical uncertainty (4.9%-50.2%), reproducibility of the measurement (1.0% for the standard sample), and systematic contribution from the measurement relative to reference materials (1.0%). As the most commonly used standard cross-section, the uncertainty of ^{93}Nb(n,2n)^{92m}Nb is approximately 1.5% [5]. The uncertainty (3.0%) of the HPGe efficiency calibration was derived from the accuracy of the calibration sources and calibration procedure. The total uncertainty was estimated using the square root of the quadratic sum of the above sources, and the overall uncertainties ranged from 7% to 50.2%.

IV. THEORETICAL CALCULATIONS

To obtain accurate and trustworthy nuclear data, theory, and experiments must be mutually verified [34–36]. Based on this, theoretical calculations for the ^{27}Al(n,2n)^{26}Al reaction were performed using the statistical nuclear reaction model codes EMPIRE-3.2.3 and TALYS-1.95 [37]. Many studies have focused on introducing these two codes, both at home and abroad [31–36], which will not be repeated in this study. Here, a brief introduction of the basic principles is provided. Computational nuclear reaction mechanisms vary depending on the energy of the incident particle [35]. These algorithms include several nuclear models that use distinct sets of optical model parameters and level densities to determine the contributions of the direct reaction (DI), pre-equilibrium emission (PE), and compound nucleus (CN). To perform theoretical calculations, the best possible input parameters must be used, which are considered to replicate the most satisfactory outcomes compared to the currently obtained data and all previous experimental data [38, 39]. In this study, cross-sections for the ^{27}Al(n,2n)^{26}Al reaction were calculated using the default parameters with an optical model (EMPIRE-3.2.3) and different level density models (TALYS-1.95). The calculated outcomes and evaluated databases are shown in Fig. 4.

V. RESULTS AND DISCUSSION

The results of the neutron energy and cross sections of the ^{27}Al(n,2n)^{26}Al reaction in the 14 MeV region are summarized in Table 3 and Fig. 7. In Fig. 7, the cross sections of the ^{27}Al(n,2n)^{26}Al reaction are compared with the available literature data in the EXFOR database. The measurements of 13–15 MeV neutron energies showed discrepancies between the data from different groups. Figure 7 shows a good agreement with the data of Wallner et al.[5] and Filatenkov et al., obtained within the experimental uncertainties. In addition, the experimental results of Zhao et al. [14] are inconsistent with the results of this study. Below the neutron energy of 14.0 MeV, the data of Sasao et al. [12] are consistent with the present data. The data of Iwasaki et al. are two times higher than the present work, between 14.0 MeV and 15.0 MeV. Compared to gamma spectrometry, the AMS technique offers a more competent method for the measurement of cross-sections of reactions with long-half-life product nuclides. Because of the short irradiation time, the statistical uncertainty of ^{26}Al became the primary source of the uncertainty source term in the experiment. If sufficient irradiation time is provided, the statistical uncertainty is greatly reduced. Without considering the AMS statistical uncertainty, the accuracy of this experiment was significantly improved. Therefore, the present results clarify the divergence of the two trends among previous experimental data, and a conclusion can be drawn as follows: the results that have a consistent trend with the present data are more accurate.

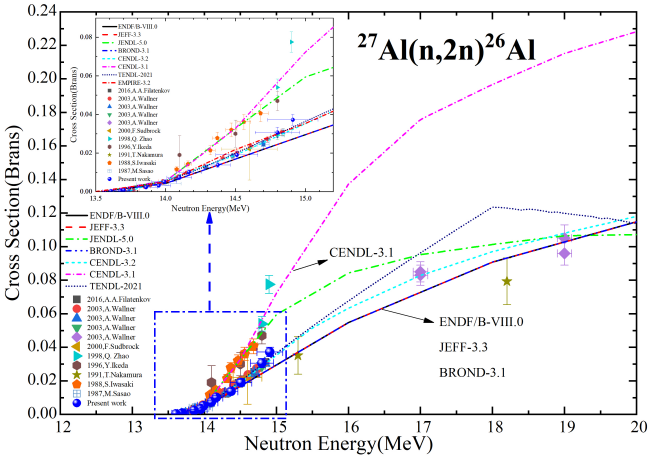

Fig. 7. (Color online) Comparison of reported cross sections of ^{27}Al(n,2n)^{26}Al reaction from threshold to 20 MeV region.

The evaluation values compiled by BROND-3.1, JEFF-3.3, ENDF/B-VIII.0, CENDL-3.2, and JENDL-5.0, are also shown in Fig. 7. The measured ^{27}Al(n,2n)^{26}Al reaction cross

TABLE 2. The uncertainty source analysis of measured ^{27}Al(n,2n)^{26}Al reaction cross section

Source of uncertainty	Uncertainty (%)
Counting statistics of ^{26}Al	4.9-50.0
Reproducibility of standard sample	∼1.0
Counting statistics of ^{92m}Nb	1.0
Half-life of ^{92m}Nb	0.2
Sample mass	0.1
Neutron flux fluctuation factor [19, 32]	3.0
Cross section of ^{93}Nb(n,2n)^{92m}Nb [5]	∼ 1.5
Standard sample (^{26}Al/^{27}Al)	1.0
Total correction factor (F)	1.0
Branching ratio	0.5
Detection efficiency	3.0
Total	6.9-50.2

TABLE 3. The present cross-section results of the ^{27}Al(n,2n)^{26}Al reaction at 14 MeV neutron energy region

Measured ratio	Neutron energy (MeV)	Neutron fluence (n/cm^2)	The ratio of ^{26}Al/^{27}Al	Cross section (mb)
1.85 ± 0.05	14.91 ± 0.18*	5.62×10^{12}	$[(2.09 \pm 0.10) \times 10^{-13}]^a$	37.20 ± 2.80
1.75 ± 0.05	14.80 ± 0.16*	3.50×10^{12}	$[(1.07 \pm 0.07) \times 10^{-13}]^a$	30.60 ± 2.72
1.60 ± 0.05	14.51 ± 0.15*	3.77×10^{12}	$[(7.18 \pm 0.59) \times 10^{-14}]^a$	19.00 ± 1.92
1.54 ± 0.05	14.37 ± 0.09	1.22×10^{13}	$[(1.69 \pm 0.14) \times 10^{-13}]^b$	13.79 ± 1.42
1.40 ± 0.05	14.17 ± 0.09	1.44×10^{13}	$[(1.46 \pm 0.13) \times 10^{-13}]^b$	10.13 ± 1.10
1.35 ± 0.05	14.10 ± 0.09	1.39×10^{13}	$[(1.01 \pm 0.16) \times 10^{-13}]^b$	7.27 ± 1.20
1.31 ± 0.04	13.99 ± 0.09*	3.46×10^{12}	$[(1.77 \pm 0.32) \times 10^{-14}]^a$	5.11 ± 0.97
1.29 ± 0.04	13.95 ± 0.09	1.46×10^{13}	$[(4.52 \pm 0.89) \times 10^{-14}]^b$	3.10 ± 0.63
1.23 ± 0.04	13.86 ± 0.08	7.10×10^{12}	$[(1.60 \pm 0.38) \times 10^{-14}]^b$	2.26 ± 0.55
1.11 ± 0.04	13.70 ± 0.07	9.68×10^{12}	$[(7.72 \pm 2.24) \times 10^{-15}]^b$	0.80 ± 0.24
1.09 ± 0.04	13.68 ± 0.07	1.25×10^{13}	$[(4.47 \pm 1.83) \times 10^{-15}]^b$	0.36 ± 0.15
1.03 ± 0.04	13.61 ± 0.06	1.42×10^{13}	$[(4.09 \pm 2.05) \times 10^{-15}]^b$	0.29 ± 0.15

Note: In the Second column, * means that the corresponding neutron energy was calculated by the theoretical method; In the third column, superscript a means they are the first set of samples, and b means that they are the second set of samples.

section falls within the range of values calculated by different models at 14 MeV neutron energy range. Our values were almost in agreement with those of CENDL-3.2. The near-threshold region above 13.5 MeV is based on different statistical model calculations and thus differs from evaluation to evaluation. The datasets of TENDL-2021 are identical and use the recent nuclear model code TALYS-1.95, where the parameters have been adjusted to reproduce the existing experimental data; however, because there is not enough experimental data to support the evaluated cross-section in the 15-20 MeV neutron energy region, there is still a divergence among the energy-dependent neutron cross-sections from the evaluated cross-section libraries JEFF-3.3, CENDL-3.2, ENDF/B-VIII.0, and JENDL-5.0. Therefore, further experimental studies are required.

In addition, the excitation function of the ^{27}Al(n,2n)^{26}Al reaction was calculated theoretically using TALYS-1.95 code and EMPIRE-3.2.3, with default parameters. In Fig. 8, the shapes of the excitation curves calculated using TALYS-1.95 (ldmodels 1-6) and EMPIRE-3.2.3 exhibit a trend similar to the present data set, which increases with increasing neutron energy around 14 MeV. However, the results calculated using ldmodel 1-6 in TALYS-1.95 significantly overestimated the excitation function. The excitation functions calculated by

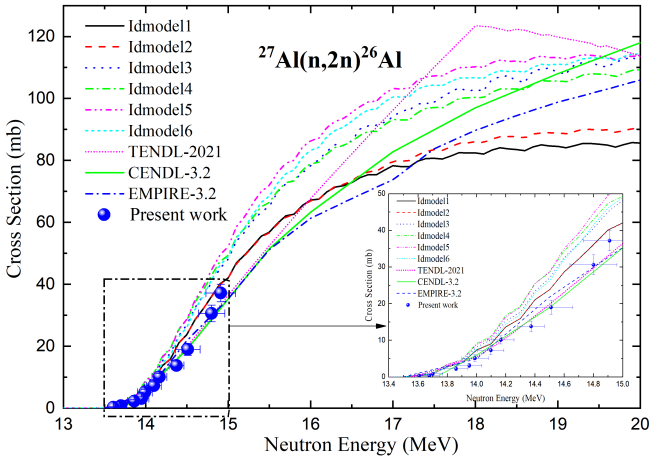

Fig. 8. (Color online) Excitation function for the ^{27}Al(n,2n)^{26}Al reaction from threshold to 20 MeV region.

the level density model ldmodel 1-2 in TALYS-1.95, are in good agreement with the experimental data compared to the level density model ldmodel 3-6. From the threshold to 15.5 MeV, EMPIRE-3.2.3 is consistent with the results reported by TENDL-2021 within the uncertainties. Therefore, more high-precision experimental data are still needed to provide parameters and an experimental basis for theoretical model calculations, especially for energy above 15.5 MeV. The present results contribute to improving the knowledge of cross-sections and optimizing the input parameters of the model, which is essential to support nuclear technology development.

VI. CONCLUSION

In order to improve the accuracy of ^{27}Al(n,2n)^{26}Al reaction cross section, neutron activation, and accelerator mass spectrometry techniques were combined to determine the ^{27}Al(n,2n)^{26}Al reaction cross section. The experiment was performed using a T(d,n)^{4}He fusion reaction-based neutron generator at CAEP. Ultrasensitive ^{26}Al analysis of the activated samples was performed using a newly installed GYIG 1MV tandem accelerator mass spectrometer. Through systematic measurement and analysis, 12 cross-sections were obtained in the 13-15 MeV neutron energy regions. A detailed analysis was performed to estimate the measured cross-sectional uncertainties. The uncertainties in the measured cross sections were in the range of 7–50%. The newly obtained cross-sections clarify the divergence among the existing experimental data, which have two different growth trends. Compared to the evaluated nuclear data, the present work is in good agreement with TENDL-2021 and CENDL-3.2. In addition, the measured cross sections were reproduced using the theoretical nuclear reaction model code EMPIRE-3.2, below 15 MeV neutron energy. The present experimental results are important for the verification of nuclear reaction codes, assessment of long-lived activity of ^{26}Al, and ion temperature diagnosis of D-T plasma in fusion reactors.

[1] F. Sudbrock, U.Herpers, S. M. Qaim et al., Cross sections for the formation of long-lived radionuclides ^{10}Be,^{26}Al and ^{36}Cl in 14.6 MeV neutron induced reactions determined via accelerator mass spectrometry (AMS). Radiochim. acta **88**, 829-832 (2000). doi: 10.1524/ract.2000.88.12.829

[2] Q. Zhao, Y. B. Nie,Y. Y. Ding et al., Measurement and simulation of the leakage neutron spectra from Fe spheres bombarded with 14 MeV neutrons.Nucl. Sci. Tech. **34**, 182 (2023). doi: 10.1007/s41365-023-01329-6

[3] R. K. Smither, L. R. Greenwood., Measurement of the ^{27}Al(n,2n)^{26}Al reaction cross section for fusion reactor applications. J. Nucl. Mater. **123**, 1071-1077(1984). doi: 10.1016/0022-3115(84)90221-6

[4] R. K. Smither, L. R. Greenwood, H. Hendel., New method for measuring ion temperatures in hot D-T plasma. Rev. Sci. Instrum. **56**, 1078-1080 (1985). doi: 10.1063/1.1138228

[5] A. Wallner, S. V. Chuvaev, A. A. Filatenkov et al., Precise measurement of the ^{27}Al(n,2n)^{26g}Al excitation function near threshold and its relevance for fusion-plasma technology. Eur. Phys. J. A **17**, 285-296 (2003). doi: 10.1140/epja/i2002-10152-3

[6] K. J. Dong, J. Q. Zhang, S. Xu, Investigation of target materials for low energy accelerator mass spectrometry of ^{26}Al. Nucl. Instru. Meth. B **515**, 14-19 (2022). doi: 10.1016/j.nimb.2022.01.006

[7] M. He, Y. N. Xu, Y. J. Guan et al., Determination of cross sections of ^{60}Ni(n,2n)^{59}Ni induced by 14 MeV neutrons with accelerator mass spectrometry. Nucl. Instru. Meth. B **361**, 517-520 (2015). doi: 10.1016/j.nimb.2015.01.060

[8] G. Z. He, B. Shi, M. He et al., Cross-section measurement for the ^{93}Nb(n,2n)^{92g}Nb reaction at the neutron energy of 14.6 MeV by the AMS method ^{26}Al. Nucl. Instru. Meth. B **42**, 074002 (2018). doi: 10.1088/1674-1137/42/7/074002

[9] T. Wright, S. Bennett, S. Heinitz et al.,Measurement of the ^{13}C(n, γ) thermal cross section via neutron irradiation and AMS. Eur. Phys. J. A **55**, 1-7 (2019). doi: 10.1140/epja/i2019-12893-0

[10] S. Jiang, Development and Application of Ultrasensitive Accelerator Mass Spectrometry. J. Chin. Mass Spectro. Soc. **40**, 401-415 (2019)(In Chinese). doi: 10.7538/zpxb.2019.0089

[11] W. Wang, X. Ruan,L. Lu et al., Absolute determination of ^{79}Se/^{80}Se with AMS. Nucl. Instru. Meth. B **268**, 764-768 (2009). doi: 10.1016/j.nimb.2009.10.025

[12] M. Sasao, T. Hayashi, K. Taniguchi et al. The cross-section of ^{27}Al(n,2n)^{26g,s}Al near 14 MeV. Phys. Rev. C **35**, 2327 (1987). doi: 1103/PhysRevC.35.2327

[13] T. Nakamura, H.Sugita, M. Imamura et al., Measurement of the long-lived ^{26}Al production cross section in the ^{27}Al(n,2n) reaction. Phys. Rev. C **43**, 4 (1991). doi:10.1103/PhysRevC.43.1831

[14] Q. Zhao, X. Lu, Z. Guo et al., Measurement of the ^{27}Al(n,2n)^{26}Al cross section using accelerator mass spectrometry. Chin. Phys. Lett. **15**, 8(1998). doi:10.1088/0256-307X/15/1/004

[15] D. A. Brown, M. B. Chadwick, R. Capote et al., ENDF/B-VIII. 0: 8th major release of the nuclear reaction data library with CIELO-project cross sections, new standards, and ther-

mal scattering data. Nucl. Data Sheets **148**, 1-142 (2018). doi: 10.1016/j.nds.2018.02.001

[16] O. Iwamoto, N. Iwamoto, S. Kunieda et al., Japanese evaluated nuclear data library version 5: JENDL-5. J. Nucl. Sci.Technol. **60**, 1-60 (2023). doi: 10.1080/00223131.2022.2141903

[17] Z. Ge, R. Xu, H. Wu et al., CENDL-3.2: The new version of Chinese general purpose evaluated nuclear data library. EPJ Web of Conferences **239**: 09001 (2020). doi: 10.1051/epjconf/202023909001

[18] A. J. M. Plompen, O. Cabellos, C. De Saint Jean et al., The joint evaluated fission and fusion nuclear data library, JEFF-3.3. Eur. Phys. J. A **56**, 181 (2020). doi: 10.1140/epja/s10050-020-00141-9

[19] I. Tetsuo, N. Kohtaro, N. Masaharu, Improvement of accuracy of Zr/Nb activation-rate ratio method for D-T neutron source energy determination. J. Nucl. Sci. Technol. **24**, 1076-1079 (1987). doi: 10.1080/18811248.1987.9733544

[20] J. Luo, L. Du, J. Zhao, A method for determining fast neutron energies in a large sample. Nucl. Instru. Meth. B **298**, 61-65 (2013). doi:10.1016/j.nimb.2013.01.029

[21] C. L. Lan, X. L. Yang, X. J. Li et al., Measurement of ^{54}Fe(n,2n)^{53}Fe reaction cross-sections at 14 MeV neutron energies using activation method and its relevance for fusion-plasma temperature diagnosis. Nucl. Instrum. Meth. B **525**, 18-24 (2022). doi: 10.1016/j.nimb.2022.06.003

[22] C. L. Lan, X. L. Yang, G. Jiang et al., An improved theoretical method for determining the mean D-T neutron energies in large solid angle sample. J. Nucl. Sci. Technol. **60**, 251-257 (2023). doi: 10.1080/00223131.2022.2093799

[23] X. Wang, S. Jiang, M. He et al. determined the cross sections for the ^{238}U(n,3n)^{236}U reaction induced by 14-MeV neutrons using accelerator mass spectrometry. Phys. Rev. C **87**, 14612 (2013). doi:10.1103/PhysRevC.87.014612

[24] H. Janssen. Spline techniques for fitting efficiency curves in gamma-ray spectrometry. Nucl. Instrum. Meth. A **286**, 398 (1990). doi:10.1016/0168-9002(90)90886-B

[25] T. Doğan, E. İlkmen, F. Kulak. A new national 1 MV AMS laboratory at TÜBİTAK MRC in Turkey. Nucl. Instrum. Meth. B **509**, 48-54 (2021). doi: 10.1016/j.nimb.2021.08.013

[26] K. Walter, Applications of accelerator mass spectrometry. Int. J. Mass Spectro. **349-350**, 203-218 (2013). doi: 10.1016/j.ijms.2013.05.023

[27] G. Gyürky, Z. Fülöp, F. Käppeler et al., The activation method for cross section measurements in nuclear astrophysics. Eur. Phys. J. A **55**, 41 (2019). doi: 10.1140/epja/i2019-12708-4

[28] Y. C. Fu, W. J. Zhou, P. Cheng et al., A New capability for ^{41}Ca analysis using CaF_3^- at the Xi'an-AMS. Nucl. Instru. Meth. B **438**, 162-165 (2018). doi: 10.1016/j.nimb.2018.05.009

[29] H. Zhang, B. Yu, L. Song et al. Preliminary progress report on ^{10}Be and ^{26}Al sample preparation at the IHEG and CAGS AMS laboratories. Nucl. Instrum. Meth. B **535**, 38-42 (2023). doi: 10.1016/j.nimb.2022.11.020

[30] W. J. Zhou, X. F. Lu, Z. K. Wu et al., New results on Xi'an-AMS and sample preparation systems at Xi'an-AMS center. Nucl. Instr. Meth. B **262**,135(2007). doi: 10.1016/j.nimb.2007.04.221

[31] C. L. Lan, Y. Zhang, T. Lv et al., Determination of neutron capture cross sections of ^{232}Th at 14.1 MeV and 14.8 MeV using the neutron activation method. Chin. Phys. C **41**, 044002 (2017). doi: 10.1088/1674-1137/41/4/044002

[32] X. Yang, C. Lan, J. Wang et al., Cross section measurements of (n, α) (n, n'α) and (n, p) reactions for ^{65}Cu at 14 MeV neutrons. Radiat. Phys. Chem. **197**, 110192 (2022). doi: 10.1016/j.radphyschem.2022.110192

[33] J. H. Luo., 14 MeV neutron physics and cross section measurement. Science Press, Beijing. 2021. ISBN:978-7-03-067073-1. (In Chinese).

[34] B. Liu, G. Tian, X. Yang et al., Activation cross sections for 13.6 MeV neutron induced reactions on natural tin. Appl. Radiat. Isotopes **184**, 110209 (2022). doi: 10.1016/j.apradiso.2022.110209

[35] Y. Wei, C. Lan, Y. Ge et al., Measurement of the half-life of ^{95m}Tc and the ^{96}Tc(n, x)^{95m}Tc reaction cross-section induced by D–T neutron with covariance analysis. Eur. Phys. J. A **58**, 222 (2022). doi: 10.1140/epja/s10050-022-00879-4

[36] J. H. Luo, J. C. Liang, L. Jiang et al.,Measurement of ^{134}Xe(n,2n)^{133m,g}Xe reaction cross-sections in 14-MeV region with detailed uncertainty quantification. Nucl. Sci. Tech. **34**, 4 (2023). doi:10.1007/s41365-022-01158-z

[37] A.J. Koning, J.P.Delaroche, Local and global nucleon optical models from 1 keV to 200 MeV. Nucl. Phys. **713**,231(2003). doi: 10.1016/S0375-9474(02)01321-0

[38] R. Capote, M. Herman, P. Obložinský et al., RIPL–reference input parameter library for calculation of nuclear reactions and nuclear data evaluations. Nucl. Data Sheets **110**, 3107-3214(2009). doi: 10.1016/j.nds.2009.10.004

[39] B. Lalremruata, N. Otuka, G. J. Tambave et al. Systematic study of (n,p) reaction cross sections from the reaction threshold to 20 MeV. Phys. Rev. C **85**, 024624 (2012).doi: 10.1103/PhysRevC.85.024624